VOLUME RECONSTRUCTION OF BREAST ECHOGRAPHY FROM ANISOTROPICALLY DEGRADATED SCANS

P. Soler and N. Villain
Philips Medical Systems Research Paris
51 rue Carnot
92156 Suresnes, France
pau.soler@philips.com

I. Bloch and E. D. Angelini
Département TSI-CNRS UMR 5141 LTCI
École Nationale Supérieure des Télécommunications
46 rue Barrault
75634 Paris Cedex, France

ABSTRACT
This paper presents a technique to reconstruct 3D breast ultrasound images at high resolution from anisotropically degradated volume acquisitions. Volumes are acquired by scanning the breast tissue with a 2D probe at different angles, showing different directional degradations induced by the point spread functions. We present a new technique to reconstruct the original volume based on estimating the spatial degradation from orthogonal views, and reconstructing the original volume through a regularized optimization technique. Results on synthetic and *in vivo* data show a better performance of this method in comparison to other spatial compounding techniques.

KEY WORDS
Breast imaging, ultrasound, reconstruction, spatial compounding.

1 Introduction

In this paper, we tackle the problem of obtaining high resolution breast volume ultrasound scans. Breast ultrasound echography, or sonography, has many benefits in comparison to other modalities, such as being non-invasive, having a good contrast resolution and being cost effective. However, it has a limited spatial resolution if we compare it to the standard x-ray mammography [4][6].

Obtaining a volume rather than two-dimensional slices permits a complete visualization of tissues, a more accurate quantification and better independency of the practitioner's use. However, echographic volume acquisition is quite challenging. Our method uses a two-dimensional probe attached to a robotic arm, which linearly scans the tissue obtaining parallel slices of the volume. This method has some drawbacks, principally the limited resolution in the elevational plane of the linear array probe. On the other hand, real three-dimensional echographic probes are still quite recent, and they have a more limited field of view, which would not suffice for this application.

We address the limited resolution problem by obtaining different scans in different directions, in order to compensate the different point spread functions. However, by having multiple volumes two new problems have to be solved: registration between the different volumes and combination of the information of each volume to reconstruct the original volume. A method for registration is proposed in [5], based on elastic registration by block matching and Thin-plate spline interpolation (see Section 2). The volume reconstruction technique from different anisotropic scans has been addressed for other modalities, such as in [7]. The novelty of our method consists in adapting this reconstruction technique to the breast sonography application. We also present a new technique to estimate the point spread function. These contributions are presented in Section 3.

In Section 4 we present the output of our technique with synthetic and *in vivo* data. Results show better tissue delineation than a volume averaging, which is the usual spatial compounding technique.

2 Acquisition and Pre-processing

2.1 Data Acquisition

All ultrasonic data have been obtained with a Philips L12-5 50 mm broadband linear array, with 192 elements and an operating range from 12 to 5 MHz. The field of view of a single two-dimensional acquisition is 5x5 cm. Volume data sets are obtained by linear scanning with a robotic arm with encoded positions. A final volume is interpolated from the two-dimensional slices, forming a volume of 5x5x5 cm for each scan.

Different scans using different orientations are obtained, namely at 0, 45, 90 and 135 degrees of the scanning direction. The system has been calibrated with a reference phantom to compensate the offsets between the different views. For this study we will limit ourselves to the use of the 0 and 90 degrees acquisitions, which we will denote as v_0 and v_{90} as short notation for $v_0(x, y, z)$ and $v_{90}(x, y, z)$.

The B-scan refers to the conventional two-dimensional ultrasound image of the volume acquired at 0 degree with respect to the scanning direction, the elevation scan refers to the perpendicular plane to the B-scan and parallel to the scanning direction, and the C-scan refers to the plane perpendicular both to the B-scan and elevational planes, as shown in Figure 1.

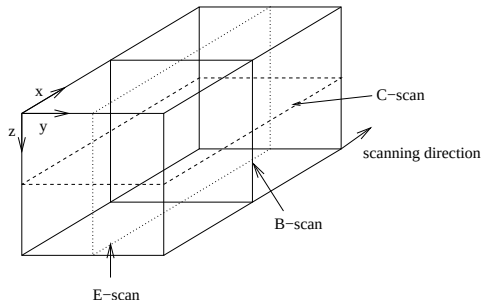

Figure 1. B-scan, C-scan, and E-scan (elevational scan)

2.2 Registration

Alignment of the volumes is necessary prior to their fusion. There are many factors which may contribute to the poor registration of the different volumes, including motion of the patient, mechanical encoding errors of the scanning device and estimation errors of the speed of sound. Different tissues may have different speeds of sound causing an error in the position of tissues when converting echo arrival times to spatial coordinates. Fusion of volumes without good alignment will lead to blur artifacts.

In order to align the volumes, a regularized block-matching algorithm described in [5] was used. It is based on a Thin-Plate spline regularization of the displacement field obtained by different block matching along the volume. We are using a block size of 5x5x5 mm and summed squared differences as similarity metric. Table 1 shows the positioning errors for a typical case. The first row shows the displacement errors before correction, and the second row after correction. The first column shows the mean displacement in the x axis, the second column in the y axis and the third in the z axis (depth), which shows to be the best registered. The fourth column shows the total mean displacement, of the order of 400 μm, which corresponds to about 2 pixels. The maximal displacement and the 90% percentile are reported in the fifth and sixth columns respectively. The registration method successfully decreased the mean displacement error and the 90% percentile error, while still some maximal errors occur, due to spurious measurements.

	dx	dy	dz	$mean$	max	$perc_{90\%}$
before	0.258	0.244	0.068	0.419	1.078	0.826
after	0.164	0.173	0.069	0.287	1.179	0.466

Table 1. Registration errors (mm)

3 Reconstruction

In order to reconstruct the original volume v from acquisitions $\tilde{v_\theta}$, we make the hypothesis that each acquisition is a version of the original volume linearly degradated by a point spread function h_θ, that is, $v_\theta = h_\theta * v$. First of all, we will model the point spread function $\tilde{h_\theta}$ and estimate model's parameters from acquisitions v_θ. We will then estimate a volume $\tilde{v}$ which best satisfies the relationship $v_\theta = \tilde{h_\theta} * \tilde{v}$ for a given set of acquisitions. In other words, we will find the volume that best estimates our acquisitions given the estimated point spread functions. To do so, we define an energy term Q which accounts for differences between the acquisitions and the estimated acquisitions, which will be minimized to obtain the optimal estimated volume $\tilde{v}$:

$$Q = \sum_\theta \left\| v_\theta - \tilde{h_\theta} * \tilde{v} \right\|^2 \quad (1)$$

As explained in section 3.2, we also define a regularization term Ψ to guarantee both the smoothness of the solution and the convergence to a global minimum. A weighting factor λ is defined to balance the contribution of the terms Q and Ψ, defining a global energy E as:

$$E = Q + \lambda \cdot \Psi \quad (2)$$

The optimal estimated volume $\tilde{v}$ is the one that minimizes energy E, $\tilde{v} = \arg\min_{\tilde{v}} E$. We use the conjugate gradient algorithm to minimize this energy, as explained in section 3.3.

3.1 Point spread function estimation

We can assume that the point spread function has an oriented Gaussian shape which depends on the acquisition depth, i.e. the z component. This assumption relies on the fact that the point spread function in the far field is theoretically the Fourier Transform of the apodization function, which in our case, is close to a Gaussian function. This assumption was corroborated for measurements on a phantom composed by small bubbles (Figure 2).

For each depth, we estimate the point spread function of v_θ by finding the equivalent Gaussian blur to the volume scanned in the perpendicular direction. This is an adapted version of the blind multichannel deconvolution technique described in [3]. For instance, to obtain the point spread function h_0, we degrade v_{90} with a Gaussian blur and we find the variance that gives the best match between v_0 and $\tilde{h_0} * v_{90}$. We denote by $v_{\theta_\perp}$ the volume acquired in a perpendicular direction. Our model contains only one parameter to estimate, which is the variance σ of the Gaussian kernel. Optimization of this parameter σ was performed with the golden search technique [2]. We have:

$$\tilde{h_\theta}(z) = \frac{1}{\sigma(z)\sqrt{2\pi}} e^{-(\vec{x_\theta})^2 / 2\sigma(z)^2} \quad (3)$$

with:

$$\sigma = \arg\min_\sigma \left\| v_\theta - \tilde{h}_\theta * v_{\theta_\perp} \right\|^2 \quad (4)$$

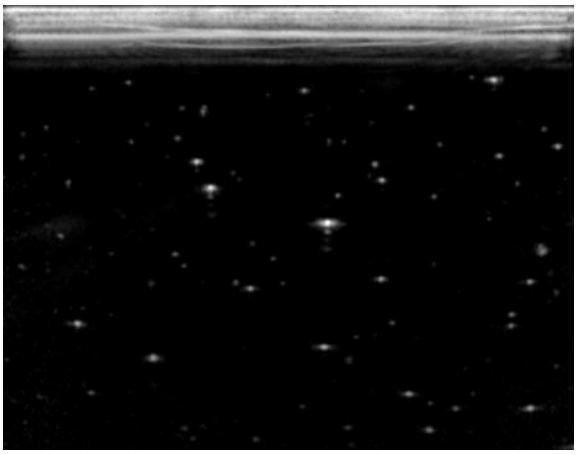

Figure 2. B-scan of bubble phantom

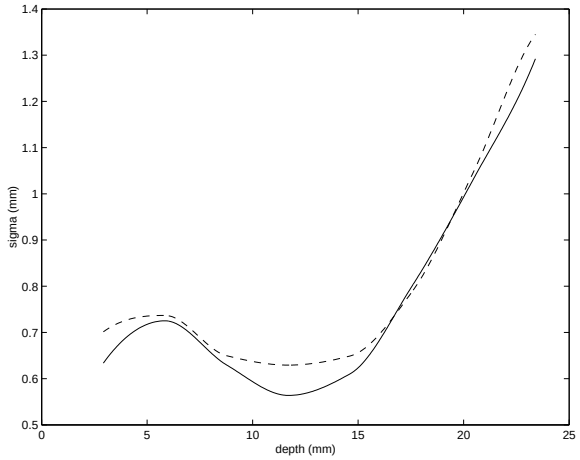

Figure 3. Elevational point spread function variance for bubble phantom (solid) and in-vivo data (dashed)

Figure 3 shows the dependency of σ with depth in the phantom and in *in vivo* data. We observe a discrepancy of about 50 μm at middle depth, but an overall good correlation.

3.2 Regularization

The reconstruction problem described in Equation 1 is an ill-posed problem. Therefore, we introduce a regularization term Ψ in order to preserve the smoothness of the final solution. It is based on the norm of some function ψ applied over the neighbor difference operator Δ_i along each dimension.

$$\begin{aligned}\Psi = &\sum_x \sum_y \sum_z \psi(\tilde{v}(x,y,z) - \tilde{v}(x-1,y,z)) + \\ &\sum_x \sum_y \sum_z \psi(\tilde{v}(x,y,z) - \tilde{v}(x,y-1,z)) + \\ &\sum_x \sum_y \sum_z \psi(\tilde{v}(x,y,z) - \tilde{v}(x,y,z-1))\end{aligned} \quad (5)$$

or in shorter notation,

$$\Psi = \|\psi(\Delta_x \tilde{v})\|_1 + \|\psi(\Delta_y \tilde{v})\|_1 + \|\psi(\Delta_z \tilde{v})\|_1 \quad (6)$$

where $\|\bullet\|_1$ represents the norm $\mathcal{L}1$.

As suggested in [7], we use a Huber function to smooth uniform areas, while preserving discontinuities. This is needed to both smooth speckle areas while preserving edges and features. A classical Tikhonov φ-function is not well suited to this application since it would also smooth discontinuities as well.

The Huber function is defined as [1]:

$$\psi(x) = \begin{cases} x^2, & \text{for } |x| \leq \alpha \\ 2\alpha\,|x| - \alpha^2, & \text{for } |x| > \alpha \end{cases} \quad (7)$$

and its derivative

$$\psi'(x) = \begin{cases} 2x, & \text{for } |x| \leq \alpha \\ 2\alpha \text{sign(x)}, & \text{for } |x| > \alpha. \end{cases} \quad (8)$$

The regularization parameter α can be seen as a threshold level where we swap from an area to be smoothed to a contour to be preserved.

The regularization parameter λ in Equation 3 controls the amount of regularization applied in the global energy E, that is, the smoothness of the final solution. The values used in this study are λ = 2.5 and α = 1.5, both tuned manually to obtain a good visual trade-off between smoothness and fine detail resolution.

3.3 Optimization

Iterative minimization of the energy was performed with the conjugate gradient approach. Although strict convexity of the energy function with this regularization term cannot be guaranteed since it depends on each image [7], we have found robust convergence with this technique. To avoid local minima, it is important to properly initialize the estimated volume $\tilde{v}$. We have chosen to initialize the system with the average of the two images, which turns out to be robust and lead to accurate results.

4 Results

4.1 Simulation

We have artificially added noise and blurred a 2D natural image to test the algorithm. In order to mimick ultrasound noise characteristics, we have added speckle noise such as $v_{noisy} = v + n \cdot v$, where n is uniformly distributed random noise with zero mean. For this experiment, we have used $var(n)$ = 0.005, which represents a peak noise of slightly more than 10% in the final images. The noisy image was blurred with an oriented Gaussian kernel at 0 and 90 degrees with a variance σ of 2, 5 and 8 pixels.

Figure 4 shows both noisy and blurred versions of the original image for $\sigma = 5$, which would represent a simulation of the acquisitions in our system, the average of these acquisitions and the reconstructed image with our algorithm. Visual inspection clearly shows superior image quality of the reconstructed image, with finer details. Root Mean Squared Error (RMSE) comparison shown in Table 2 corroborates the improvement of the technique for different degradation levels.

σ(pixels)	v_0	v_{90}	v_{avg}	v_{rec}
2	17.86	14.69	13.95	8.33
5	25.08	21.98	20.99	11.71
8	29.73	26.76	25.46	16.67

Table 2. Root Mean Squared Error for simulation data, for speckle noise $var(n)$=0.005.

4.2 In-vivo data

Figure 5 shows a C-scan of a breast tissue for the 0 degree acquisition, the 90 degrees acquisition, the average and the reconstructed volume. The 0 degree acquisition has been acquired by scanning the ultrasound probe from top to bottom of the image, therefore we can see vertical blur due to the limited elevational resolution. On the other hand, with the 90 degrees acquisition, which has been obtained from left to right, we see an horizontal blur. The average volume does not show a predominant direction of blur, and smoothes out the speckle noise. However, edges are also blurred turning into poor tissue delineation and lack of details. The reconstructed volume shows a better resolution with finer details.

Figure 6 shows a B-scan of a breast tissue. It corresponds to a B-scan of the 0 degree acquisition, providing highest image quality we are expecting. The 90 degrees acquisition is blurred by the limited elevation resolution. The average volume shows a resolution level slightly better than the 90 degrees acquisition, but not as good as the 0 degree acquisition. Speckle is smoothed out, but some of the finer details are also smoothed out. The reconstructed volume shows a better resolution and tissue delineation, preserving the resolution of the 0 degree acquisition.

On the other hand, Figure 7 shows an elevational scan of the breast tissue. It corresponds to a B-scan of the 90 degrees acquisition, that is, the same case as the B-scan but interchanging the place between the 0 degree and the 90 degrees acquistions. Here again, the average volume shows poor resolution but good speckle attenuation, while the reconstructed volume shows better tissue delineation.

Figure 4. Image with synthetic degradation. From top to bottom: 1. Acquisition at 0 degree, 2. Acquisition at 90 degrees, 3. Average, 4. Reconstructed volume

5 Conclusions

We have presented a system which overcomes the limited elevational resolution by acquiring multiple volumes at different angles and reconstructing a single data set from these acquisitions. The reconstructed data preserve the features of individual acquisitions while successfully maintaining the best spatial resolution of each acquisition, reducing spatial degradation. This leads to better tissue delineation and finer details. Volume reconstruction also cancels out uncorrelated structures such as speckle. Comparing to volume averaging, we observed that on large areas, speckle reduction is apparently better filtered by a simple averaging. We can foresee to combine these two techniques, averaging in speckle areas and the reconstructed volume in the detail areas.

References

[1] M.J. Black and A. Rangarajan. On the unification of line process, outlier rejection, and robust statistics with applications in early vision. *Internat. J. Comput. Vision*, 19(1):57–91, 1996.

[2] M. A. Malcolm Forsythe, G. E. and C. B. Moler. *Computer Methods for Mathematical Computations*. Prentice-Hall, 1976.

[3] G. Harikumar and Y. Bresler. Perfect blind restoration of images blurred by multiple filters: theory and efficient algorithms. *IEEE Transactions on Image Processing*, 8(2):202–219, February 1999.

[4] Tina J. Hieken, Jacqueline Harrison, Jose Herreros, and Jose M. Velasco. Correlating sonography, mammography, and pathology in the assessment of breast cancer size. *The American Journal of Surgery*, 182(4):351–354, October 2001.

[5] J. F. Krücker, G. L. LeCarpentier, J. B. Fowlkes, and P. L. Carson. Rapid elastic image registration for 3-d ultrasound. *IEEE Transactions on Medical Imaging*, 21:1384 – 1394, November 2002.

[6] S.K. Moore. Better breast cancer detection. *Spectrum, IEEE*, 38(5):50–54, May 2001.

[7] E. Roullot, A. Herment, I. Bloch, A. de Cesare, M. Nikolova, and E. Mousseaux. Modeling anisotropic undersampling of magnetic resonance angiographies and reconstruction of a high-resolution isotropic volume using half-quadratic regularization techniques. *Signal Processing*, 84(4):743–762, April 2004.

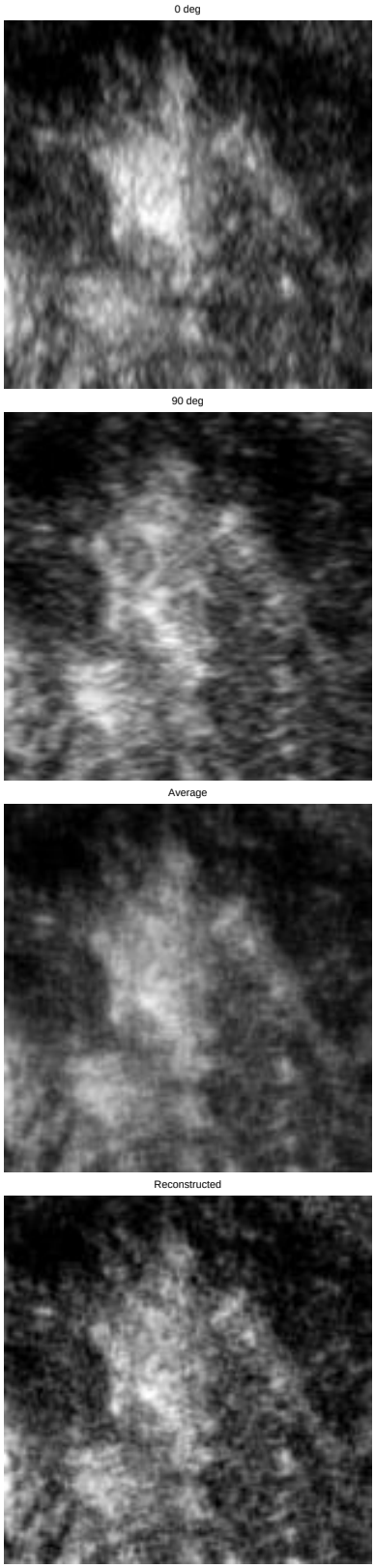

Figure 5. C-scan. From top to bottom: 1. Acquisition at 0 degree, 2. Acquisition at 90 degrees, 3. Average volume, 4. Reconstructed volume

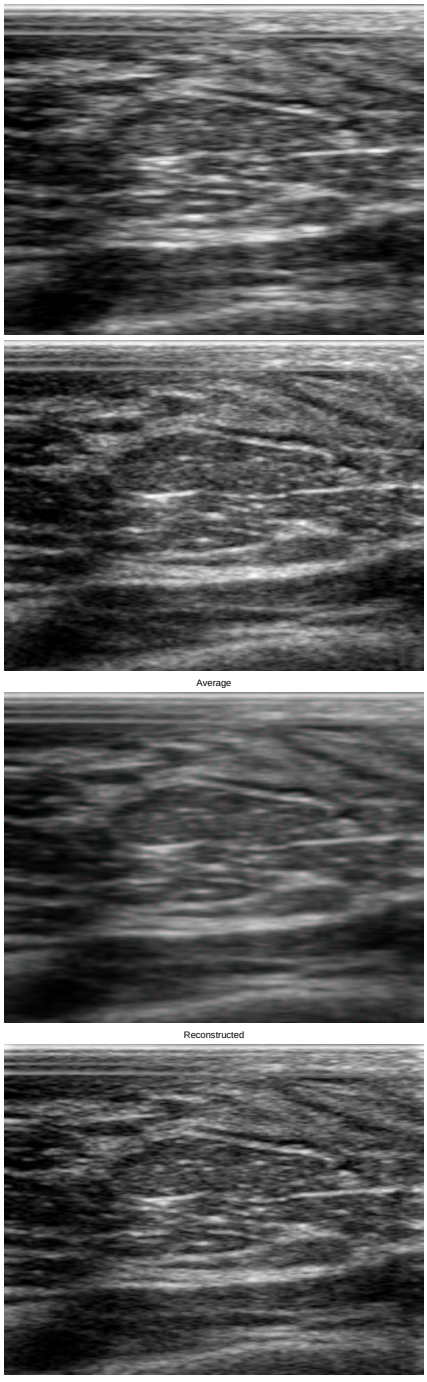

Figure 6. B-scan. From top to bottom: 1. Acquisition at 0 degree, 2. Acquisition at 90 degrees, 3. Average volume, 4. Reconstructed volume

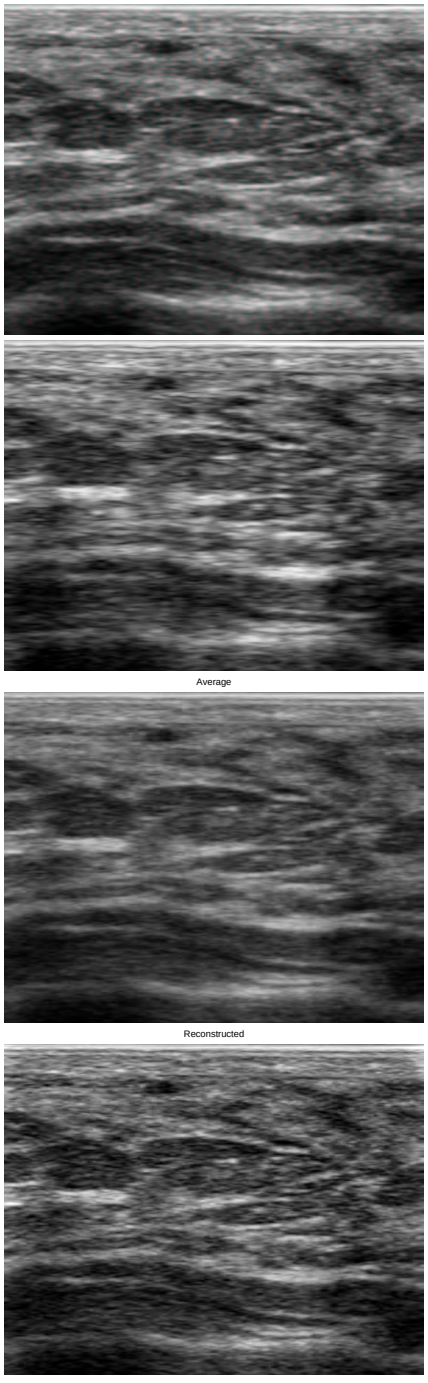

Figure 7. Elevation scan. From top to bottom: 1. Acquisition at 0 degree, 2. Acquisition at 90 degrees, 3. Average volume, 4. Reconstructed volume